THE JOURNAL OF PHYSICAL CHEMISTRY Letters

pubs.acs.org/JPCL Letter

Visualizing the Geometry of Hydrogen Dimers

Arnab Khan, Till Jahnke, Stefan Zeller, Florian Trinter, Markus Schöffler, Lothar Ph. H. Schmidt, Reinhard Dörner,* and Maksim Kunitski

Cite This: J. Phys. Chem. Lett. 2020, 11, 2457−2463 Read Online

ACCESS | Metrics & More | Article Recommendations | Supporting Information

ABSTRACT: The simplest molecular dimer, H_2-H_2, poses a challenge to both experiment and theory as a system with a multidimensional energy surface that supports only a single weakly bound quantum state. Here, we provide a direct experimental image of the structure of hydrogen dimers [$(H_2)_2$, H_2-D_2, and $(D_2)_2$] obtained via femtosecond laser-induced Coulomb explosion imaging. Our results indicate that hydrogen dimers are not restricted to a particular geometry but rather occur as a mixture of all possible configurations. The measured intermolecular distance distributions were used to deduce the isotropic intermolecular potential as well as the binding energies of the dimers.

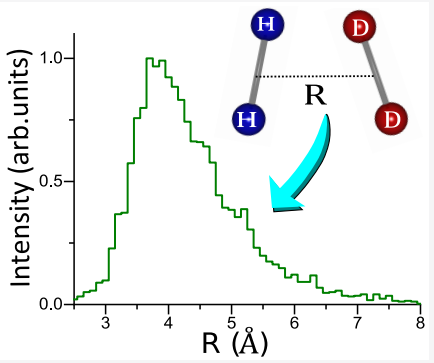

The hydrogen molecule (H_2) and the helium atom (He) are the two simplest, two-electron systems that have attracted an enormous amount of attention of the research community over the past few decades. Despite being very weakly polarizable, both species can form clusters under sufficiently cold conditions. The smallest clusters, dimers (consisting of either two hydrogen molecules or two helium atoms), are very fragile and support only one vibrational bound state.[1−15] The helium dimer, which has a tiny binding energy (E_{bind}) of only 1.7 mK, has a wave function that 80% resides in the classically forbidden tunneling region and, thus, belongs to a class of systems categorized as quantum halos.[13] In contrast, the hydrogen dimer is known to be more tightly bound (E_{bind} = 3−4 K). Theoretical work on the interaction between two hydrogen molecules started in the early 1940s[16−18] and was motivated by the fundamental nature of the hydrogen dimer. *Ab initio* studies of such systems are, however, rather challenging, because they require an accuracy of approximately 1 K in the calculation of the potential energy surfaces (PES), implying the use of large basis sets with dispersive wave functions and time-consuming quantum chemistry methods such as the coupled-cluster technique. Additional complexity arises from the multidimensionality of the problem.[10,11,19] One of the fundamental questions is still a matter of dispute, whether the interaction between two hydrogen molecules in the dimer is of a dispersive or electrostatic nature.[20]

Theoretically, the six-dimensional PES of the hydrogen dimer comprises several local minima and transition points. They correspond to different geometrical structures such as parallel (H-shaped), perpendicular (X-shaped), linear (L-shaped), slipped-parallel or rhombohedral (Z-shaped), and T-shaped (see Figure 1 for the schematic).[7,10,12,20−22] Among these, the T and Z configurations are predicted to be the most stable, whereas the L-shaped configuration is the least stable.[20] Specifically, the Z configuration is a transition-state structure between two T structures [T_1 and T_2 for heterodimers (cf. Figure 1)] with a very low potential barrier.[12,23] These structures, however, cannot be considered as different conformers in a common sense, i.e., being related to different quantum states, because the intermolecular potential of the hydrogen dimer supports only one single bound state and the energy of this state is higher than the barriers separating the various potential minima. Nevertheless, the six-dimensional probability density should reflect the differences in the potential energies among different structures.

With respect to experimental work, Watanabe and Welsh reported on the laboratory-based spectroscopic evidence of bound states of the hydrogen dimer in the early 1960s.[1] Subsequent studies, employing infrared spectroscopy, were conducted by McKellar and co-workers.[9,24,25] They allowed identification of the presence of the hydrogen dimer in the atmospheres of Jupiter and Saturn.[26] Recently, the hydrogen dimer was found on the other giant planets of our solar system.[27]

The intermolecular potential of the hydrogen dimers has been mainly addressed by measuring the differential[28−30] and

Received: March 3, 2020
Accepted: March 9, 2020
Published: March 9, 2020

https://dx.doi.org/10.1021/acs.jpclett.0c00702
J. Phys. Chem. Lett. 2020, 11, 2457−2463

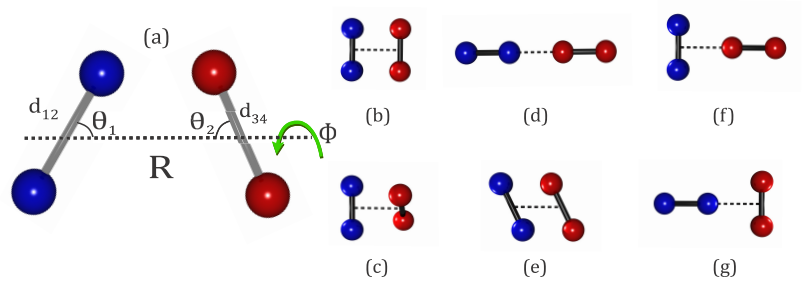

Figure 1. (a) Definition of the hydrogen dimer structure. θ_1 ($0° \le \theta_1 \le 90°$) and θ_2 ($0° \le \theta_2 \le 180°$) are the angles with respect to the dimer axis. Φ ($-90° \le \Phi \le 90°$) is the azimuthal (or torsional) angle between the two monomers (all of the angles are in degrees). Here, d_{12} and d_{34} are the bond lengths of the first and second monomer, respectively, and R is the intermolecular distance. (b–g) Schematics of different possible geometries of the dimer: (b) parallel (H-shaped), (c) perpendicular (X-shaped), (d) linear (L-shaped), (e) slipped-parallel (Z-shaped), (f) T_1-shaped, and (g) T_2-shaped. These T_1 and T_2 configurations are especially important for the heterodimer, like H_2-D_2. H_2 perpendicular to R is termed T_1, while H_2 parallel to R is termed T_2.

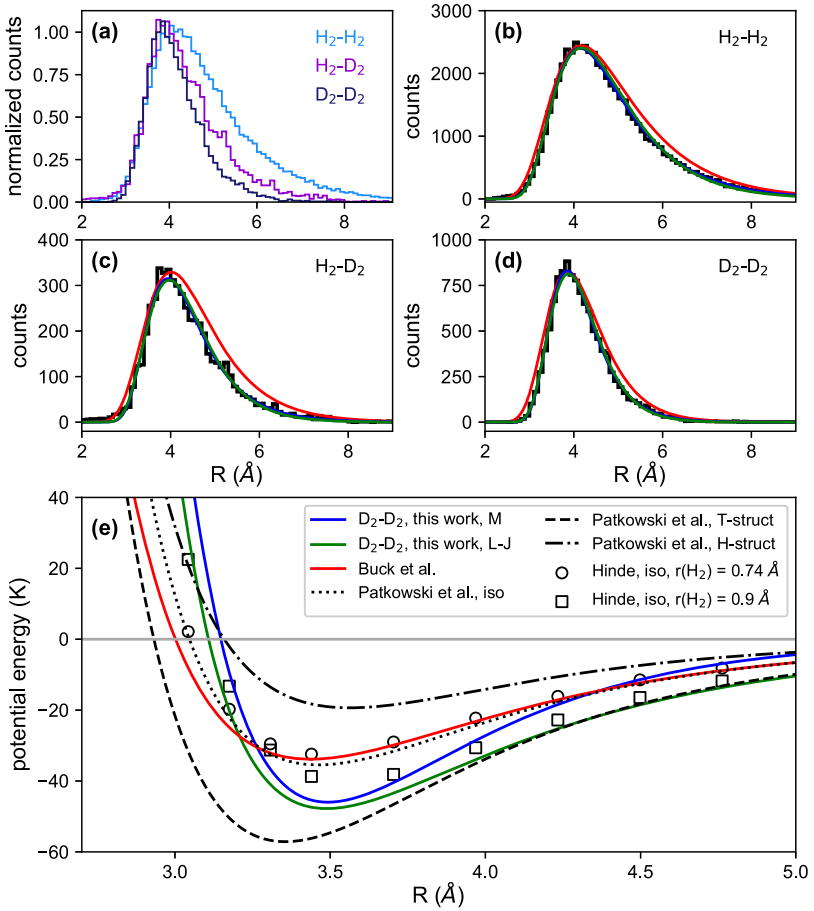

Figure 2. (a) Measured intermolecular distance distributions for $(H_2)_2$, H_2-D_2, and $(D_2)_2$. In panels b–d, black represents measured, blue and green represent fitted simulations employing Morse (M) and Lennard-Jones (L-J) potentials, respectively, and red represents simulations using the isotropic potential from Buck et al.[30] The intermolecular potentials are presented in panel e. Blue and green lines are fitted Morse and Lennard-Jones potentials yielding the distributions in panel d [for the fitted potentials of $(H_2)_2$ and H_2-D_2, see the Supporting Information]. Black dotted, dashed, and dashed–dotted lines are the calculated isotropic, T structure, and H structure potentials, respectively, from Patkowski et al.[19] Circles and squares correspond to the calculated isotropic potentials from Hinde[11] with H–H bond lengths of 0.74 and 0.9 Å, respectively.

integral[31−33] scattering cross sections in molecular beam experiments. Being extremely sensitive to the repulsive part of the potential, scattering experiments provide, however, less information about the attractive region. In this study, we use a completely different experimental approach to reveal the intermolecular potential and geometrical structures of the hydrogen dimer. The approach is based on Coulomb explosion imaging (CEI), which is implemented within a cold-target recoil-ion momentum spectroscopy (COLTRIMS) reaction microscope.[15,34−37] CEI is a technique that offers the ability to image an instantaneous structure of a single molecule. Thus, by Coulomb-exploding a large number of molecules in the gas phase, it allows the square of the wave function to be sampled without having any beforehand knowledge of the system.[15,34,38,39] Knowing the wave function, in turn, allows one to obtain the corresponding potential energy surfaces by

https://dx.doi.org/10.1021/acs.jpclett.0c00702
J. Phys. Chem. Lett. 2020, 11, 2457−2463

inverting the Schrödinger equation.[40] The applicability of CEI to "floppy" van der Waals systems was discussed decades ago by Vager et al.[39] for accelerator-based CEI of molecular ions. Neutral species can today be Coulomb-exploded by stripping of the electrons by short and strong laser pulses.[15,34,41]

Our study mainly concentrates on the H_2-D_2 heterodimer and partially on the $(H_2)_2$ and $(D_2)_2$ homodimers. We chose this mixed dimer system for a practical reason: the CEI of a symmetric system like $(H_2)_2$ and $(D_2)_2$ is technically challenging as such systems consist of four equal particles, which makes the interpretation of the acquired momentum space data more complicated. Therefore, the use of H_2-D_2 makes the analysis and understanding of the experimental data much more straightforward and unambiguous. Additionally, the knowledge acquired from the H_2-D_2 study helps us to analyze the fragmentation of the $(D_2)_2$ system, which is discussed in the Supporting Information. For the $(H_2)_2$ dimer, only two-body fragmentation has been considered.

First, we produce the hydrogen dimers by means of a supersonic expansion of a 50:50 mixture of *normal*-H_2 (a 3:1 *ortho*:*para* ratio) and *normal*-D_2 (a 2:1 *ortho*:*para* ratio) through a 5 μm nozzle. The nozzle is precooled to a temperature of 35 K. The dimer yield is optimized by adjusting the nozzle pressure to 1.3 bar. We use the matter–wave diffraction technique to obtain a pure H_2-D_2 and $(D_2)_2$ beam from the mixture of all monomers and higher clusters occurring in the supersonic gas jet.[15,42,43] In brief, due to the mass difference, different dimers, which all travel with the same velocity in the gas jet, can be spatially separated, as the diffraction angle depends on their de Broglie wavelengths. The $(H_2)_2$ dimer cannot be separated by this approach as the mass of $(H_2)_2$ is the same as that of D_2. Therefore, the $(H_2)_2$ dimer has been measured in a separate experiment under the same experimental conditions. We use circularly polarized 30 fs laser pulses with a central wavelength of 780 nm and a repetition rate of 8 kHz for ionization of the dimers. The peak intensity of the laser field (I_0) is estimated to be $\sim 2 \times 10^{15}$ W/cm^2. The intensity is chosen such that ionization mostly happens within the rising edge of the laser pulse.[44] By interacting with the laser beam, the dimers are multiply ionized and, subsequently, Coulomb-exploded. The three-dimensional momenta of all singly charged ions upon breakup of a single dimer have been measured in coincidence using COLTRIMS.[35−37] We use a homogeneous electric field of 19.5 V/cm to guide the ions onto a time- and position-sensitive detector with hexagonal delay-line position readout.[45]

The intermolecular distance distribution of the hydrogen dimers is retrieved from the two-body fragmentation channels: $(H_2)_2^{2+} \rightarrow H_2^+ + H_2^+$, $(D_2)_2^{2+} \rightarrow D_2^+ + D_2^+$, and $(H_2\text{-}D_2)^{2+} \rightarrow H_2^+ + D_2^+$ (Figure 2a). In all cases, the ionization and fragmentation happen very fast compared to any intermolecular motion. Therefore, the kinetic energy of two molecular ions [kinetic energy release (KER)] acquired upon Coulomb explosion of the dimer is equal to the initial potential energy $1/R$ (in atomic units). Thus, by measuring the KER, one can deduce the intermolecular distance (R) at the instant of ionization. Repeating such measurements on many individual dimers provides the intermolecular distance distribution (or the effective isotropic one-dimensional squared wave function) of the hydrogen dimers. The distributions yield mean intermolecular distances of 4.93, 4.39, and 4.15 Å for $(H_2)_2$, H_2-D_2, and $(D_2)_2$, respectively.

We used several types of analytical potentials, namely, Morse,[46] Lennard-Jones ("12-6"),[47] and Buckingham ("exp-6"),[48] to reproduce the experimental intermolecular distance distributions. These distributions were obtained by solving the time-independent one-dimensional Schrödinger equation numerically using the Numerov algorithm. The potential parameters were optimized by fitting the simulated intermolecular distributions to the measured ones. The resulting "best-fit" potentials, as well as the corresponding probability distributions, are shown in Figure 2b–e. The optimized potential parameters are listed in Table 1. All of the potentials

Table 1. Potential Parameters, Corresponding χ^2 Values, and Binding Energies of $(H_2)_2$, H_2-D_2, and $(D_2)_2$[a]

	V_{min} (K)	R_{min} (Å)	E_{bind} (K)	χ^2
	H_2-H_2			
Buck et al.,[30] iso	33.9	3.44	–	–
Patkowski et al.,[19] iso	35.45	3.46	–	–
Patkowski et al.,[19] T structure	57.12	3.35	–	–
Patkowski et al.,[19] Z structure	52.94	3.38	–	–
Patkowski et al.,[19] H structure	19.36	3.56	–	–
	H_2-H_2, This Work			
Morse	43(2)	3.50(2)	4.4(2)	74.1
Buckingham ("exp-6")	47(3)	3.40(3)	5.4(2)	148.1
Lennard-Jones ("12-6")	42(1)	3.43(2)	5.8(2)	201.3
	H_2-D_2, This Work			
Morse	49(6)	3.47(5)	8(2)	57.9
Buckingham ("exp-6")	52(9)	3.42(7)	10(2)	66.0
Lennard-Jones ("12-6")	47(3)	3.45(3)	11(2)	73.0
	D_2-D_2, This Work			
Morse	46(3)	3.49(3)	11(2)	37.8
Buckingham ("exp-6")	49(3)	3.46(4)	14(2)	47.5
Lennard-Jones ("12-6")	48(2)	3.49(2)	16(2)	59.3

[a]The uncertainties of the fitted parameters are shown in parentheses.

can accurately reproduce the measured intermolecular distance distributions, but the Morse potential results in the lowest χ^2 deviation. For comparison, we show also the isotropic potential obtained by Buck et al.[30] with the corresponding $|\Psi(R)|^2$ distributions of the dimers (Figure 2b–d, red). As one can see, the Buck potential yields intermolecular distance distributions that are generally broader than the measured ones, indicating the lower depth and broader width of the Buck potential. Because our approach relies on the measured intermolecular distance distribution, the obtained potentials are only relevant in the region of intermolecular distances covered by this distribution, i.e., in the region of the potential well. The repulsive part of the intermolecular potential should be much more accurate in Buck's potential, which was derived by fitting scattering cross sections.

The "best-fit" potentials found in this work are also deeper than the theoretical isotropic potentials from Patkowski et al.[19] (Figure 2e, black dotted line) and Hinde[11] with the H–H bond of 0.74 Å (Figure 2e, circles). The obtained potential well depths lie between the theoretical isotropic one and that corresponding to the T structure (Figure 2e, dashed line). One possible explanation for this might be as follows. The measured one-dimensional intermolecular distance distribution, which is used to obtain an effective isotropic one-dimensional potential energy, is a projection of the full six-dimensional probability distribution to the intermolecular coordinate R. The deeper regions of the six-dimensional potential should yield higher

https://dx.doi.org/10.1021/acs.jpclett.0c00702
J. Phys. Chem. Lett. 2020, 11, 2457−2463

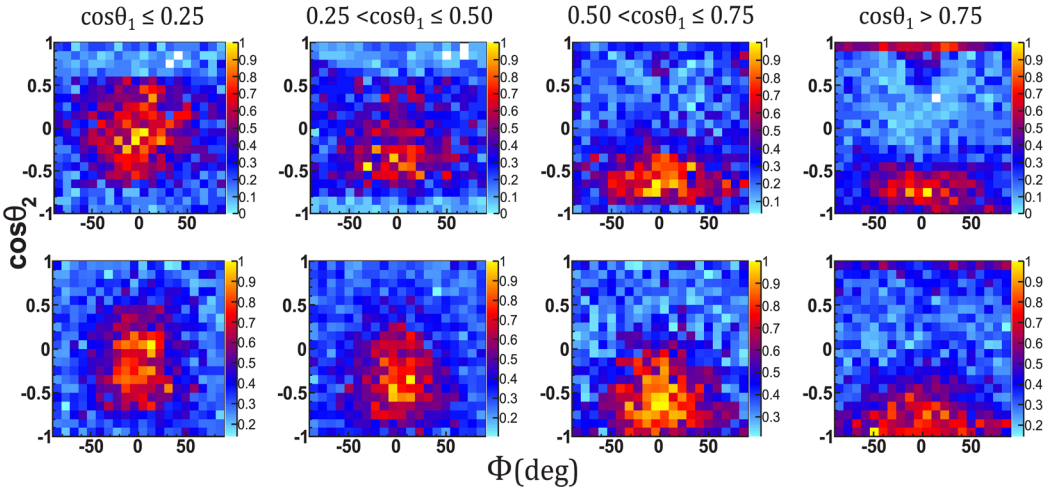

Figure 3. Geometry of the dimer (for definition of angles, see Figure 1a). The top row shows the experimental results for H_2-D_2: angles in coordinate space from numerical inversion of the measured momenta to the initial positions (see the text). The data are strongly influenced by the selective ionization probability of the strong laser field (see the text and comparison with the bottom row). The bottom row shows the distribution from the simulated Coulomb explosion starting with a random dimer geometry in coordinate space, including the weighting by the angular dependence of the strong-field double ionization probability.

local probability density and, thus, have a larger contribution (weighting) to the measured intermolecular distance distribution. In turn, the one-dimensional potential deduced from such a distribution should be deeper than an unweighted isotropic potential. In addition, the fitted simulation of the intermolecular distance distribution provides the binding energies of the dimers. In contrast to parameters such as the depth of the potential well V_{min} and the equilibrium intermolecular distance R_{min}, the binding energy depends strongly on the potential type used in the simulation. For $(H_2)_2$, it ranges from 4.4 K (Morse) to 5.8 K (Lennard-Jones). The bindings are successively stronger in the case of H_2-D_2 (8−11 K) and $(D_2)_2$ (11−16 K) due to the higher reduced masses.

Furthermore, if we compare the distance distributions presented here with those of other weakly bound dimers such as Ne_2, Ar_2, and He_2, some significant differences can be observed. In the case of Ne_2 or Ar_2, the internuclear distance distributions are quite narrow and symmetric,[49] while for He_2, the distribution is very broad and has a long tail spreading toward larger distances.[13] The reason for this is that Ne_2 and Ar_2 dimers are more tightly bound than are He_2 dimers, whose ground state is located near the dissociation continuum, resulting in tunneling of a large portion of its wave function into the classically forbidden region. The hydrogen dimers' distributions are between those of Ar_2 and He_2, showing the onset of the tail on the right. The tail in the distribution becomes larger with a decrease in the reduced mass of the dimer [from $(D_2)_2$ to $(H_2)_2$ (Figure 2a)] for two reasons. First, as the lighter dimers have a higher zero-point vibrational energy, the anharmonicity of the potential leads to an asymmetric broadening of the intermolecular distribution. Second, the lighter systems tunnel deeper into the classically forbidden region, because the tunneling probability depends on the mass and the barrier height (i.e., binding energy).[13,42]

Moreover, to understand the three-dimensional (3D) spatial distribution, we consider the four-body decay of quadruply ionized dimers, $(H_2\text{-}D_2)^{4+} \rightarrow H^+ + H^+ + D^+ + D^+$. We reconstruct the spatial geometry of each dimer from the measured momenta by performing a numerical inversion of the Coulomb explosion process (see the Supporting Information for the details). Though the reconstruction yields all six internal coordinates of the dimer [d_{12}, d_{34}, R, θ_1, θ_2, and Φ (Figure 1a)], we consider only the angles, because they alone are already sufficient for determination of the structure type. Here, θ_1 ($0° \le \theta_1 \le 90°$) and θ_2 ($0° \le \theta_2 \le 180°$) are the angles of the monomer axis with respect to the intermolecular axis and Φ ($-90° \le \Phi \le 90°$) is the dihedral angle.[10,20] In Figure 3, we depict the two-dimensional distributions of cos θ_2 versus Φ for different cos θ_1 ranges. These distributions, however, do not directly show the spatial distributions of the unperturbed dimer. This is because the 4-fold ionization probability in the laser field, in contrast to the 2-fold ionization discussed above, depends on the spatial orientation of the dimer with respect to the laser-polarization direction, resulting in a preferred selection of certain dimer geometries during CEI. The main effect that causes this orientation-dependent ionization rate is so-called enhanced ionization (EI).[50] For a diatomic molecule, the double ionization probability in a strong laser field is enhanced by orders of magnitude for particular internuclear distances when the electric field points along the molecular axis and drops rapidly for other orientations. Consequently, when two constituent monomers of a dimer both lie within the polarization plane, the total ionization probability is maximized. This condition is more frequently satisfied for H, Z, and L structures than for T_1 and T_2 geometries. The nonplanar X structure has, thus, the lowest ionization probability. To obtain information about the unweighted populations of different dimer structures, we performed a simulation of the 4-fold ionization of randomly oriented dimers. For this, we used the measured angular ionization dependencies of H_2 and D_2 molecules that were measured within the same experiment. The simulated cos θ_2−Φ distributions for different cos θ_1 ranges of random structures (meaning all of the structures are equally probable) are shown in the bottom row of Figure 3. The simulated distributions resemble well the experimental ones (top row of Figure 3), suggesting that all structures of the H_2-D_2 dimer are equally probable within our experimental resolution.

Another approach to eliminate orientation-dependent ionization weighting is to consider only the dimers that lay

https://dx.doi.org/10.1021/acs.jpclett.0c00702
J. Phys. Chem. Lett. 2020, 11, 2457−2463

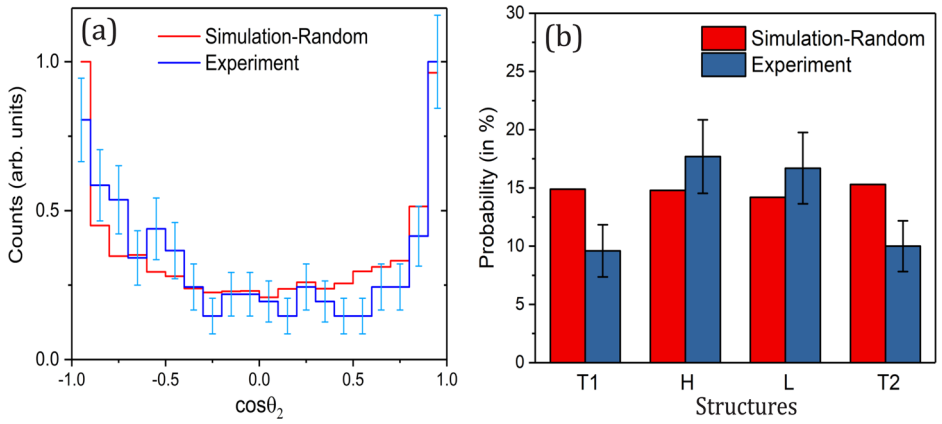

Figure 4. (a) Experimental and simulated distribution of cos θ_2 for events where all momentum vectors are within the light's polarization plane. For the simulation, a random spatial geometry of the dimer was initialized. (b) Classification of spatial structures for events where all momentum vectors are in the polarization plane of the circularly polarized laser pulse. The X structure is excluded by definition due to the planar geometry. Additionally, the Z structures ($\theta_1 \approx \theta_2$) and some intermediate structures (various θ_1 and θ_2 combinations) are not considered, which contribute to missing ~40% of counts in the simulation. Error bars shown here correspond to the statistical errors of the data.

upon ionization in the polarization plane of the laser light. As we use circularly polarized light, the ionization probability for different dimer structures located within this plane should be equal. This approach works, however, only for planar geometries and, thus, cannot be applied to the X structure. For this subset of the data, we show the one-dimensional experimental cos θ_2 distribution in Figure 4a. The simulated distribution for random structures (Figure 4a, red) shows good resemblance to the experimental result, confirming the equal presence of all considered structures. Despite low statistics, we tried to assign the reconstructed dimer structures by gating on different areas of the cos θ_1−cos θ_2 space. In this space, for instance, the structure around cos $\theta_1 \approx 0$ and cos $\theta_2 \approx 0$ corresponds to the H structure ($\theta_1 \approx 90°$, and $\theta_2 \approx 90°$). The corresponding distribution is shown in Figure 4b along with that of randomly oriented dimers. This analysis also shows that all H_2-D_2 structures are equally probable in our experiment.

In summary, we applied laser-induced Coulomb explosion imaging to study the structure and the intermolecular potential of the hydrogen dimers. The Coulomb explosion resulting in the four-body fragmentation reveals that, to a large extent, all structures are equally possible, which is in line with the statement of McKellar that "the dimers do not have a meaningful molecular structure or geometry in the usual sense".[8] The two-body Coulomb explosion of the dimer yields isotropic intermolecular distance distributions. A fitted simulation of these distributions by solving the time-independent Schrödinger equation provides the isotropic intermolecular potential energy binding the two hydrogen molecules. Because our approach relies on structural imaging, the obtained potentials are only accurate in the regions of the potential well, where the wave function is non-zero. Moreover, in the case of multidimensional potential energy surfaces, the resulting isotropic potentials are weighted by the probability density. The isotropic potentials of the hydrogen dimers obtained in this work are systematically deeper than those obtained from theory and by molecular scattering experiments. One possible explanation for this could be the population weighting of the deeper potential regions, corresponding to T and Z structures. We hope that these results will serve as a benchmark for further theoretical studies.

■ ASSOCIATED CONTENT

Supporting Information

A detailed description of the experimental setup, calibration of the ion detector via Ar_2 Coulomb explosion, determination of the intermolecular potential from intermolecular distances, details of the structure reconstruction from measured momenta, and last, determination of the D_2 dimer's structure from four-body decay. The Supporting Information is available free of charge at https://pubs.acs.org/doi/10.1021/acs.jpclett.0c00702.

(ZIP)

(PDF)

■ AUTHOR INFORMATION

Corresponding Author

Reinhard Dörner − *Institut für Kernphysik, Goethe-Universität 60438 Frankfurt, Germany*; Email: doerner@atom.uni-frankfurt.de

Authors

Arnab Khan − *Institut für Kernphysik, Goethe-Universität 60438 Frankfurt, Germany*; orcid.org/0000-0002-1343-8031

Till Jahnke − *Institut für Kernphysik, Goethe-Universität 60438 Frankfurt, Germany*

Stefan Zeller − *Institut für Kernphysik, Goethe-Universität 60438 Frankfurt, Germany*

Florian Trinter − *Institut für Kernphysik, Goethe-Universität 60438 Frankfurt, Germany*

Markus Schöffler − *Institut für Kernphysik, Goethe-Universität 60438 Frankfurt, Germany*

Lothar Ph. H. Schmidt − *Institut für Kernphysik, Goethe-Universität 60438 Frankfurt, Germany*

Maksim Kunitski − *Institut für Kernphysik, Goethe-Universität 60438 Frankfurt, Germany*

Complete contact information is available at: https://pubs.acs.org/10.1021/acs.jpclett.0c00702

Notes

The authors declare no competing financial interest.

https://dx.doi.org/10.1021/acs.jpclett.0c00702
J. Phys. Chem. Lett. 2020, 11, 2457−2463

■ ACKNOWLEDGMENTS

A.K. acknowledges support by the Alexander von Humboldt Foundation. The authors acknowledge support from Deutsche Forschungsgemeinschaft via Sonderforschungsbereich 1319 (ELCH).

■ REFERENCES

(1) Watanabe, A.; Welsh, H. L. Direct Spectroscopic Evidence of Bound States of $(H_2)_2$ Complexes at Low Temperatures. *Phys. Rev. Lett.* **1964**, *13*, 810−812.
(2) Ewing, G. E. Intermolecular Interactions: van der Waals Molecules. *Angew. Chem., Int. Ed. Engl.* **1972**, *11*, 486−495.
(3) Danby, G.; Flower, D. R. Theoretical Studies of van der Waals Molecules: the H_2 -H_2 Dimer. *J. Phys. B: At. Mol. Phys.* **1983**, *16*, 3411−3422.
(4) Danby, G. Theoretical Studies of van der Waals Molecules: the D_2 -D_2 Dimer. *J. Phys. B: At., Mol. Opt. Phys.* **1989**, *22*, 1785−1807.
(5) Kochanski, E. Evaluation of the Intermolecular Energy Between Two Hydrogen Molecules Near the van der Waals Minimum, From a Perturbative Procedure. *J. Chem. Phys.* **1973**, *58*, 5823−5831.
(6) Ree, F. H.; Bender, C. F. Repulsive Intermolecular Potential Between Two H_2 Molecules. *J. Chem. Phys.* **1979**, *71*, 5362−5375.
(7) Burton, P. G.; Senff, U. E. The $(H_2)_2$ Potential Surface and the Interaction Between Hydrogen Molecules at Low Temperatures. *J. Chem. Phys.* **1982**, *76*, 6073−6087.
(8) McKellar, A. R. W. Infrared Spectra of Hydrogen Dimers. *J. Chem. Phys.* **1990**, *92*, 3261−3277.
(9) McKellar, A. R. W.; Schaefer, J. Far-infrared Spectra of Hydrogen Dimers: Comparisons of Experiment and Theory for $(H_2)_2$ and $(D_2)_2$ at 20 K. *J. Chem. Phys.* **1991**, *95*, 3081−3091.
(10) Diep, P.; Johnson, J. K. An Accurate H_2−h_2 Interaction Potential From First Principles. *J. Chem. Phys.* **2000**, *112*, 4465−4473.
(11) Hinde, R. J. A Six-dimensional H_2−H_2 Potential Energy Surface for Bound State Spectroscopy. *J. Chem. Phys.* **2008**, *128*, 154308.
(12) Carmichael, M.; Chenoweth, K.; Dykstra, C. E. Hydrogen Molecule Clusters. *J. Phys. Chem. A* **2004**, *108*, 3143−3152.
(13) Zeller, S.; Kunitski, M.; Voigtsberger, J.; Kalinin, A.; Schottelius, A.; Schober, C.; Waitz, M.; Sann, H.; Hartung, A.; Bauer, T.; et al. Imaging the He_2 Quantum Halo State Using a Free Electron Laser. *Proc. Natl. Acad. Sci. U. S. A.* **2016**, *113*, 14651−14655.
(14) Grisenti, R. E.; Schöllkopf, W.; Toennies, J. P.; Hegerfeldt, G. C.; Köhler, T.; Stoll, M. Determination of the Bond Length and Binding Energy of the Helium Dimer by Diffraction from a Transmission Grating. *Phys. Rev. Lett.* **2000**, *85*, 2284−2287.
(15) Voigtsberger, J.; Zeller, S.; Becht, J.; Neumann, N.; Sturm, F.; Kim, H.-K.; Waitz, M.; Trinter, F.; Kunitski, M.; Kalinin, A.; et al. Imaging the Structure of the Trimer Systems $^4He_3$ and $^3He^4He_2$. *Nat. Commun.* **2014**, *5*, 5765.
(16) Margenau, H. The Forces Between Hydrogen Molecules. *Phys. Rev.* **1943**, *63*, 385−386.
(17) Evett, A. A.; Margenau, H. The Forces between Hydrogen Molecules. *J. Chem. Phys.* **1953**, *21*, 958−959.
(18) Mason, E. A.; Rice, W. E. The Intermolecular Potentials of Helium and Hydrogen. *J. Chem. Phys.* **1954**, *22*, 522−535.
(19) Patkowski, K.; Cencek, W.; Jankowski, P.; Szalewicz, K.; Mehl, J. B.; Garberoglio, G.; Harvey, A. H. Potential Energy Surface for Interactions Between Two Hydrogen Molecules. *J. Chem. Phys.* **2008**, *129*, No. 094304.
(20) Lu, T.; Chen, F. Revealing the Nature of Intermolecular Interaction and Configurational Preference of the Nonpolar Molecular Dimers $(H_2)_2$, $(N_2)_2$, and $(H_2)(N_2)$. *J. Mol. Model.* **2013**, *19*, 5387−5395.
(21) Tapia, O.; Bessis, G. Intermolecular Interactions-dependence on Inter- and Intramolecular Distances. A Configuration Interaction Study of the H_2...H_2 System. *Theoret. chim. Acta* **1972**, *25*, 130−137.
(22) Donchev, A. G.; Galkin, N. G.; Tarasov, V. I. Anisotropic Nonadditive Ab Initio Force Field for Noncovalent Interactions of H_2. *J. Chem. Phys.* **2007**, *126*, 174307.
(23) Schneider, B.; Hobza, P.; Zahradník, R. Potential Energy Surface of the $(H_2)_2$ Dimer: an MP2 Study. *Theoret. chim. Acta* **1988**, *73*, 201−206.
(24) McKellar, A. R. W.; Welsh, H. L. Spectra of $(H_2)_2$, $(D_2)_2$, and H_2−D_2 van der Waals Complexes. *Can. J. Phys.* **1974**, *52*, 1082−1089.
(25) McKellar, A. R. W. Long-Path Equilibrium IR Spectra of Weakly Bound Complexes at Low Temperatures. *Faraday Discuss.* **1994**, *97*, 69−80.
(26) McKellar, A. R. W. Experimental Verification of Hydrogen Dimers in the Atmospheres of Jupiter and Saturn from Voyager IRIS Far-Infrared Spectra. *Astrophys. J.* **1988**, *326*, L75−L77.
(27) Fletcher, L. N.; Gustafsson, M.; Orton, G. S. Hydrogen Dimers in Giant-Planet Infrared Spectra. *Astrophys. J.* **2018**, *235*, 24.
(28) Dondi, M.; Valbusa, U.; Scoles, G. Energy Dependence of the Differential Collision Cross Section for Hydrogen at Thermal Energies. *Chem. Phys. Lett.* **1972**, *17*, 137−141.
(29) Farrar, J. M.; Lee, Y. T. Intermolecular Potentials from Crossed Beam Differential Elastic Scattering Measurements. VII. para-H_2+para-H_2. *J. Chem. Phys.* **1972**, *57*, 5492−5497.
(30) Buck, U.; Huisken, F.; Kohlhase, A.; Otten, D.; Schaefer, J. State Resolved Rotational Excitation in D_2+H_2 Collisions. *J. Chem. Phys.* **1983**, *78*, 4439−4450.
(31) Butz, H. P.; Feltgen, R.; Pauly, H.; Vehmeyer, H. Totale Effektive Streuquerschnitte Für Die Streuung von He, HD Und D_2 an Verschiedenen Molekülen. *Z. Phys. A: Hadrons Nucl.* **1971**, *247*, 70−83.
(32) Gengenbach, R.; Hahn, C.; Schrader, W.; Toennies, J. P. Determination of the H_2-H_2 Potential from Absolute Integral Cross Section Measurements. *Theoret. Chim. Acta (Berl.)* **1974**, *34*, 199−212.
(33) Bauer, W.; Lantzsch, B.; Toennies, J.; Walaschewski, K. Observation of Symmetry Undulations in the Integral Cross Section of para-H_2 (J = 0)+para-H_2 (J = 0), and the Determination of the Attractive Potential. *Chem. Phys.* **1976**, *17*, 19−26.
(34) Pitzer, M.; Kunitski, M.; Johnson, A. S.; Jahnke, T.; Sann, H.; Sturm, F.; Schmidt, L. P. H.; Schmidt-Böcking, H.; Dörner, R.; Stohner, J.; et al. Direct Determination of Absolute Molecular Stereochemistry in Gas Phase by Coulomb Explosion Imaging. *Science* **2013**, *341*, 1096−1100.
(35) Ullrich, J.; Moshammer, R.; Dörner, R.; Jagutzki, O.; Mergel, V.; Schmidt-Böcking, H.; Spielberger, L. Recoil-ion Momentum Spectroscopy. *J. Phys. B: At., Mol. Opt. Phys.* **1997**, *30*, 2917−2974.
(36) Dörner, R.; Mergel, V.; Jagutzki, O.; Spielberger, L.; Ullrich, J.; Moshammer, R.; Schmidt-Böcking, H. Cold Target Recoil Ion Momentum Spectroscopy: a 'momentum Microscope' to View Atomic Collision Dynamics. *Phys. Rep.* **2000**, *330*, 95−192.
(37) Jahnke, T.; Weber, T.; Osipov, T.; Landers, A. L.; Jagutzki, O.; Schmidt, L. P. H.; Cocke, C. L.; Prior, M. H.; Schmidt-Böcking, H.; Dörner, R. Multicoincidence Studies of Photo and Auger Electrons From Fixed-in-space Molecules Using the COLTRIMS Technique. *J. Electron Spectrosc. Relat. Phenom.* **2004**, *141*, 229−238.
(38) Gemmell, D. S. Determining the Stereochemical Structures of Molecular Ions by "coulomb-explosion" Techniques With Fast (MeV) Molecular Ion Beams. *Chem. Rev.* **1980**, *80*, 301−311.
(39) Vager, Z.; Naaman, R.; Kanter, E. P. Coulomb Explosion Imaging of Small Molecules. *Science* **1989**, *244*, 426−431.
(40) Zeller, S.; Kunitski, M.; Voigtsberger, J.; Waitz, M.; Trinter, F.; Eckart, S.; Kalinin, A.; Czasch, A.; Schmidt, L. P. H.; Weber, T.; et al. Determination of Interatomic Potentials of He_2, Ne_2, Ar_2, and H_2 by Wave Function Imaging. *Phys. Rev. Lett.* **2018**, *121*, No. 083002.
(41) Chelkowski, S.; Corkum, P. B.; Bandrauk, A. D. Femtosecond Coulomb Explosion Imaging of Vibrational Wave Functions. *Phys. Rev. Lett.* **1999**, *82*, 3416−3419.
(42) Kunitski, M.; Zeller, S.; Voigtsberger, J.; Kalinin, A.; Schmidt, L. P. H.; Schöffler, M.; Czasch, A.; Schöllkopf, W.; Grisenti, R. E.;

https://dx.doi.org/10.1021/acs.jpclett.0c00702
J. Phys. Chem. Lett. 2020, 11, 2457−2463

Jahnke, T.; et al. Observation of the Efimov State of the Helium Trimer. *Science* **2015**, *348*, 551−555.
(43) Kornilov, O.; Toennies, J. P. Electron Impact Ionization of Size Selected Hydrogen Clusters $(H_2)_N$: Ion Fragment and Neutral Size Distributions. *J. Chem. Phys.* **2008**, *128*, 194306.
(44) Posthumus, J. H.; Plumridge, J.; Taday, P. F.; Sanderson, J. H.; Langley, A. J.; Codling, K.; Bryan, W. A. Sub-pulselength Time Resolution of Bond Softening and Coulomb Explosion Using Polarization Control of Laser-induced Alignment. *J. Phys. B: At., Mol. Opt. Phys.* **1999**, *32*, L93−L101.
(45) Jagutzki, O.; Cerezo, A.; Czasch, A.; Dörner, R.; Hattaß, M.; Huang, M.; Mergel, V.; Spillmann, U.; Ullmann-Pfleger, K.; Weber, T.; et al. Multiple Hit Readout of a Microchannel Plate Detector With a Three-layer Delay-line Anode. *IEEE Trans. Nucl. Sci.* **2002**, *49*, 2477−2483.
(46) Morse, P. M. Diatomic Molecules According to the Wave Mechanics. II. Vibrational Levels. *Phys. Rev.* **1929**, *34*, 57−64.
(47) Jones, J. E.; Chapman, S. On the Determination of Molecular Fields. II. From the Equation of State of a Gas. *Proc. R. Soc. London, Ser. A* **1924**, *106*, 463−477.
(48) Buckingham, R. A.; Lennard-Jones, J. E. The Classical Equation of State of Gaseous Helium, Neon and Argon. *Proc. R. Soc. London, Ser. A* **1938**, *168*, 264−283.
(49) Ulrich, B.; Vredenborg, A.; Malakzadeh, A.; Schmidt, L. P. H.; Havermeier, T.; Meckel, M.; Cole, K.; Smolarski, M.; Chang, Z.; Jahnke, T.; et al. Imaging of the Structure of the Argon and Neon Dimer, Trimer, and Tetramer. *J. Phys. Chem. A* **2011**, *115*, 6936−6941.
(50) Légaré, F.; Litvinyuk, I. V.; Dooley, P. W.; Quéré, F.; Bandrauk, A. D.; Villeneuve, D. M.; Corkum, P. B. Time-Resolved Double Ionization with Few Cycle Laser Pulses. *Phys. Rev. Lett.* **2003**, *91*, No. 093002.

https://dx.doi.org/10.1021/acs.jpclett.0c00702
J. Phys. Chem. Lett. 2020, 11, 2457−2463